Experimental Study on Kaiser Effect of Reinforced Concrete Simply-Supported Beams

Yongfeng XU, Hailong WANG, Tengfei HE*, Jiajun MA, Pengfei ZHAO, Anquan JI, Lei LIU, Yang LIU

Abstract: With the progress of transportation, an increasing number of bridges are put into operation, and the assessment of bridge bearing capacity is considered a significant measure to ensure bridge safety. As a critical approach for structural monitoring, acoustic emission is widely used in engineering projects. Since the Kaiser effect is an important phenomenon in acoustic emission, it is necessary to explore the Kaiser effect of reinforced concrete structures and the determination method of the Kaiser point. In this thesis, four reinforced concrete simply supported beams were utilized for the graded loading experiment under bending loads. After accumulating acoustic emission parameters, Kaiser point was selected for preliminary evaluation. Taking Kaiser point as the midpoint, the appropriate interval was determined. According to the continuity criterion of acoustic emission signals and the quadratic fitting curve based on experimental data, the Kaiser point was corrected by following the average growth rate of acoustic emission parameters. These simply supported beams were classified into two groups. One group was used to explore the acoustic emission characteristics when the load was less than the historical maximum, while the other group was used to analyze changes in the Kaiser effect with increasing load. Finally, based on the results of the specimen inspection, the influence of initial damage on the Kaiser effect was analyzed. The research results alleviated the influence of human factors on the determination of the Kaiser point and can serve as the theoretical basis for damage monitoring based on the Kaiser effect and bearing capacity evaluation of reinforced concrete structures.

Keywords: acoustic emission; felicity ratio; kaiser effect; reinforced concrete; simply-supported beamu

1 INTRODUCTION

Acoustic emission (AE) is a physical phenomenon widely existing in nature. When an object is deformed or damaged under load, the potential energy accumulated in the object is released in the form of elastic wave, which is the phenomenon of AE [1-4]. Acoustic emission waves come from the structure itself, so dynamic information of structural damage can be obtained, and the location, degree and category of structural damage can be assessed based on this [5, 6]. In the 1950s, Kaiser, a German scientist, found that when the load did not reach the historical maximum value of the load on the material, the material would not produce obvious acoustic emission phenomenon [7, 8]. Such irreversible phenomenon of acoustic emission is called Kaiser effect. Kaiser effect has laid a foundation for the application of acoustic emission in the field of engineering. For a long time, Kaiser effect and its mechanism have become the focus of people's research.

Research on Kaiser effect began with metal materials. Rusch and Mccabeetal found in their research that Kaiser effect also exists in brittle materials such as concrete and rock [9-11]. Takeshi-watanabe found in his study that the Kaiser effect of concrete is correlated with strength, and the higher the strength of concrete is, the more obvious the Kaiser effect will be [12]. When studying the relationship between the Kaiser effect and Felicity effect of concrete materials, Ji Hongguang et al. found that the Kaiser effect of concrete materials is related to the stress level. There are upper limit of stress (70% - 80% of the ultimate stress) and lower limit (30% - 40% of the ultimate stress), and the upper limit of stress depends on the failure mechanism of the material. The lower limit of stress depends on the structural characteristics of the material itself [13]. Researches on Kaiser effect of concrete mainly focus on AE characteristics of materials themselves under different loads [14-17]. The research of reinforced concrete beam mainly focuses on the acoustic emission characteristics of the whole process of concrete beam failure. Men et al. [18] conducted the four-point bending experiment and acoustic emission test on reinforced concrete simply supported

beams, obtained the change law of acoustic emission parameters such as amplitude and energy with load, and identified the initial cracking and steel yield of the components. Fan et al. [19] conducted the three-point bending experiment on model beams, clarified the influence of factors such as concrete strength and reinforcement ratio on the acoustic characteristics of the model beam according to ring-down count and cumulated ring-down count, as well as energy and cumulative energy, and identified cracking and instability loads. Yu [20] adopted the correlation distribution map of acoustic emission rise time and amplitude to characterize the damage process of reinforced concrete model beams, evaluated the damage based on the Kurtosis criterion, and identified typical failure stages by means of neural network technology. Chen [21] clarified the fracture damage law through a three-point bending test of concrete beams and achieved the classification of crack modes based on Gaussian mixture modeling. Rasheed et al. [22] conducted crack initiation and propagation acoustic emission tests on model beams clarified the changes in cumulative acoustic emission energy with load and sound power density, conducted three-dimensional source localization, and found that the crack source location identified by acoustic emission was consistent with the actual crack development by analyzing the acoustic emission results. Nguyen-Tat et al. [23] utilized acoustic emission technology to explore the degradation mechanism of concrete beams under bending loads, evaluated the degree of damage based on the static load ratio classification method, obtained results that were highly consistent with the mechanical test result, analyzed the acoustic emission waveform and determined the acoustic emission source. Shi [24] has studied the acoustic emission characteristics of high strength concrete, and the results show that the use of acoustic emission characteristics to judge the damage stage of concrete is consistent with the reality. Shield [25] found in her research on concrete beams that concrete beams have obvious Kaiser effect under bending load. Ge et al. [26] pointed out in their study that the Kaiser effect was strictly effective in the low stress stage of reinforced concrete

beams, and the Felicity effect became more obvious as the stress increased. At present, there are relatively few researches on Kaiser effect of reinforced concrete beams, Kaiser point, the recovery of effective AE judgment is inconclusive. In this paper, a method of correcting the Kaiser point using quadratic fitting curves based on experimental data was explored through the four-point bending experiment and signal continuity criterion. The effects of different loads and initial defects on reinforced concrete beams at the Kaiser point were analyzed.

2 EXPERIMENTAL PROCESS AND PHENOMENA
2.1 Specimen Preparation

Before the experiment, four beams for the experiment were poured as required, and were denoted as No. 1 beam to No. 4 beam respectively. The specimens were cast with artificially mixed concrete of C25 strength. The cement is 32.5 grade ordinary Portland cement produced by Jidong Cement of China, the sand is medium sand, the stone is gravel (maximum particle size 10 mm), the mixing water is tap water, and the concrete mix ratio is cement: sand: stone: water = 1:1.57:2.79:0.5. The reinforcement is made of 4 HRB335 hot-rolled ribbed steel bars with diameter of 12 mm as the main reinforcement and the frame reinforcement, the ultimate tensile strength is 510 N/mm² and the yield strength is 335 N/mm². The stirrups are made of HPB235 plain round steel bars of $\varphi 8@100$, the ultimate tensile strength is 310 N/mm² and the yield strength is 235 N/mm². The size of the specimen is 1400 mm × 100 mm × 160 mm, and the thickness of the reinforcement protection layer is 20 mm, as shown in Fig. 1. The beams were cast with steel formwork and the concrete was poured in two parts. After the steel skeleton is in place, about 1/2 height concrete is first poured into the formwork, and a vibrating rod with a diameter of 2.5 cm is used to vibrate. After it is compacted, the concrete is poured again and vibrated until it meets the requirements. The concrete experimental beam was finished on May 11, 2021. The weather forecast temperature of that day was 11 – 25 °C, which was suitable for concrete pouring. After pouring, the specimens were placed in the shade for watering and curing for 28 days, and placed in the open air in the natural environment for about 4 months. The experiment was started on October 24, 2021. Before the experiment, the SCL-MATS B multi-functional nondestructive detector for concrete was used to detect the defects of the specimen. The detection methods were impact echo method and elastic wave CT method, the detailed detection process and results are as follows.
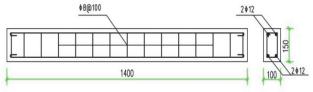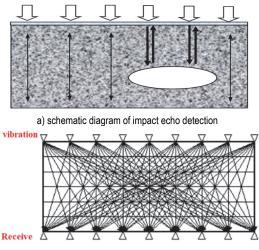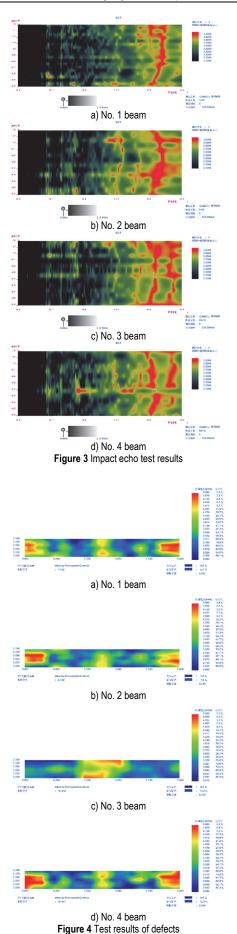

Figure 1 Design diagram of reinforced concrete beam

The impact echo method is the most effective method in one sided reflection method. During the test, the elastic wave signal is continuously excited along the surface of the test object, and the signal will be reflected when it encounters porous medium such as cavity. By extracting the reflected signal and conducting corresponding image processing, the internal defects of the structure can be identified, as shown in Fig. 2a. Tomography scanning (CT) is a nondestructive testing technique based on shock elastic wave, which is used to detect the interior of concrete members by double-face scanning method. When there are weak areas or defects in the test area, the elastic wave signal will generate diffraction when propagating in the concrete, and the propagation time will be longer. The wave velocity in the test area will be reduced by the inverse calculation of the computer chromatography technology. Therefore, the internal quality of concrete structure can be detected by wave velocity distribution and evaluation criteria, as shown in Fig. 2b when the field test, impact echo method and elastic wave CT method were used in this test. With the impact echo method, measuring lines are arranged along the length, with the intervals of measuring points being 0.1 m, and tested from north to south (0 - 1.4 m). The layout of survey line is shown in Fig. 2.

a) schematic diagram of impact echo detection

b) schematic diagram of chromatographic scanning (CT) detection
Figure 2 Detection method diagram

The test results of impact echo method showed that no obvious defects were found in No. 1 and No. 2 beams, No. 3 beam was slightly uncompact at about 0.65 m, and No. 4 beam was uncompact at about 0.5 m, as shown in Fig. 3. The cloud image of sound velocity using tomography (CT) is shown in Fig. 4. Beam No. 1 (Fig. 4a) has the lowest sound velocity (2.587 km/s) at the lower edge of the beam at 0.45 m and at the upper edge and lower edge of the beam at 0.9 m. Beam No. 2 (Fig. 4b) has a minimum sound speed of 2.5 km/s, which is less than 2.56 km/s. There are serious defects, which appear at the upper edge of beam 0.9 m in length. Beam No. 3 (Fig. 4c) has a minimum sound speed of 2.57 km/s and beam No. 4 (Fig. 4d) has the lowest sound velocity of 2.56 km/s, which appears at 0.9 m in the long direction of beam. The signal processing software of the concrete multifunctional nondestructive detector was used to analyze the distribution and proportion of sound velocity (Fig. 4).

a) No. 1 beam

b) No. 2 beam

c) No. 3 beam

d) No. 4 beam

Figure 3 Impact echo test results

a) No. 1 beam

b) No. 2 beam

c) No. 3 beam

d) No. 4 beam

Figure 4 Test results of defects

The CT results showed that no obvious defects were found in No. 1 beam, and the proportion of suspected

defects was about 5.4%; No. 2 beam had serious defects, and the proportion of suspected defects was about 1%, and the proportion of suspected defects was about 7.9%; No. 3 beam had serious defects, and the proportion of suspected defects was about 11.9%; No. 4 beam had serious defects, and the proportion of suspected defects was 0.8%, as shown in Fig. 4. In the figure, color represents wave velocity, red represents high wave velocity, and blue represents low wave velocity. The calibrated P-wave velocity is 3.2 km/s as the judging benchmark, lower than 20% is considered as a serious defect.

2.2 Experimental Scheme

The experiment was carried out with Beijing Soft Island ds5-8B full information acoustic emission signal analyzer; acoustic emission signals are collected using 8 acoustic emission sensors of model RS-2A. The position coordinates of the sensor take beam length direction as axis X, beam width direction as axis Y, and beam height direction as axis Z, as shown in Fig. 5. The detailed coordinate values are shown in Tab. 1.

Table 1 Sensor detail coordinates

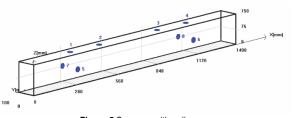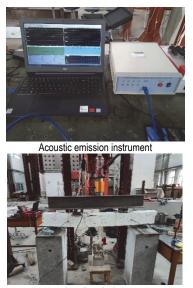| Sensor	No. 1	No. 2	No. 3	No. 4	No. 5	No. 6	No. 7	No. 8
X	300	500	900	1100	300	1100	300	1100
Y	50	50	50	50	0	0	100	100
Z	150	150	150	150	75	75	75	75

Figure 5 Sensor position diagram

During the experiment, a 20 ton manual jack was used in the loading device, and a 200 kN pressure sensor was used in the force measuring device. The loading system was formed by the jack, pressure sensor and steel reaction frame, as shown in Fig. 6.

Acoustic emission instrument

Loading device

Figure 6 Experimental instruments and loading devices

The four-point bending loading method was adopted in the acoustic emission experiment. The calculated span of the simply supported beam was 1200 mm, and the pure bending section was 600 mm, as shown in Fig. 7. The loading process of each specimen is cyclic loading in stages and sections until the specimen is damaged. After the damage, the residual bearing capacity of the beam body is continued to be loaded and its AE signal is collected. The AE information is not collected during the unloading process after the completion of each stage of loading.
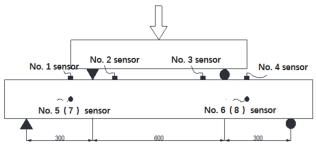

Figure 7 Schematic diagram of loading mode

2.3 Experimental Process and Phenomena

Before the experiment, the four specimens were calibrated by lead-break experiment. Two sensors were arranged at two sections of 200 mm and 1000 mm along the side of the beam for calibration. The lead-break position was selected at 400 mm and 800 mm, and lead-break was performed three times at the corresponding section for each calibration. The sound velocity of each beam was calibrated three times and the average of the three velocities is used as the sound velocity of the beam. The speed of sound of beams No. 1 to No. 4 is 2618 m/s, 2479 m/s, 2575 m/s and 2483 m/s respectively.

In order to reduce the influence of mechanical friction on acoustic emission data, a rubber pad is set between the support and beam phase to reduce the noise isolation. The environmental noise was collected and analyzed before the experiment began. The amplitude of environmental noise was generally lower than 40 dB, and combined with literature [26] the threshold value of data collection was set as 40 dB, the transmission gain is set to 40 dB, and the hardware analog filter is set to straight-through [27]. Peak distinguish time (PDT) was 300 µs, hit distinguish time (HDT) was 650 µs, and hit locking time (HLT) was 800 µs [28]. According to the calculation of the design parameters and loading position of the beam, the maximum load that

the beam can bear is 50 kN, and 20%, 30% and 50% of the maximum load of each beam are used as the first load.
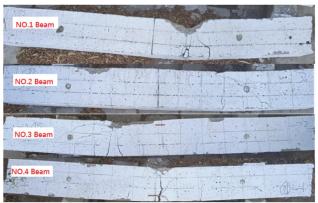

Figure 8 Diagram of experimental beam failure

During the experiment, No. 1 beam was loaded to 80kN under the fourth load, and the experimental bending speed increased. The load continued to rise no longer, so it was judged that the beam had been destroyed. And then, the damaged beam was loaded twice, and the maximum load reached 60 kN and 55 kN respectively. When the fourth load of No. 2 beam was loaded to 89 kN, the deflection of the beam increased, and the load stopped when it was difficult to increase. When the fifth load was loaded, the maximum value reached 95 kN, which was judged as the failure of the beam. After that, the damaged specimens were loaded twice, reaching 92 kN and 87 kN respectively. No. 3 beam was damaged when the fourth load was loaded to 87 kN. After unloading, the specimen was loaded with the fifth load, and the maximum load was 59 kN. No. 4 beam was damaged when the fifth grade load reached 55.5 kN. After that, the damaged beam was loaded twice, with a load value of 52 kN and 50 kN respectively, the loading details of each beam are shown in Tab. 2. The failure forms of each experimental beam body are shown in Fig. 8, in which No. 1, 3 and 4 beams show obvious failure in the compression zone, and No. 4 beam has serious cracks in the middle span, with the widest crack reaching about 10mm. Compared with other beams, No. 2 beam has obvious shear cracks. Experiments show that the ultimate bearing capacity of No. 4 beam is much smaller than that of No. 1 to No. 3 beam. Field observation shows that the effective height of No. 4 beam is significantly reduced because of the reinforcement cage layout of the beam is tilted to one side.

Table 2 Experiment beam loading process

Beam	Level 1 / kN	Level 2 / kN	Level 3 / kN	Level 4 / kN	Level 5 / kN	Level 6 / kN	Level 7 / kN
No. 1	0 - 45	0 - 30	0 - 30	0 - 80	0 - 60	0 - 55	/
No. 2	0 - 45	0 - 30	0 - 35	0 - 89	0 - 95	0 - 92	0 - 87
No. 3	0 - 16.6	0 - 25	0 - 42	0 - 87	0 - 59	/	/
No. 4	0 - 11	0 - 21	0 - 31	0 - 41	0 - 55.5	0 - 52	0 - 50

3 DATA PROCESSING AND THE KAISER EFFECT ANALYSIS

3.1 Parameter Selection and Kaiser Point Determination

During the experiment, data were collected and stored in the form of full-parameter waveform files, which were subsequently processed in the analytical process.

Parametric analysis is an important analytical method in acoustic emission tests, with different parameters reflecting different aspects of acoustic emission characteristics. Examining the Kaiser effect requires the determination of the effectiveness of the acoustic emission signals based on the analysis of the degree of intensity of acoustic emission activities. Parameters reflecting the
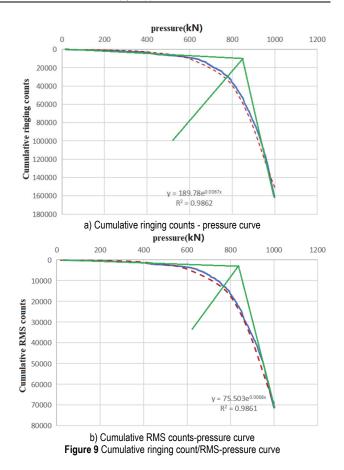
degree of intensity of acoustic emission mainly include hit, event-count, ringing-count, energy and root-mean-square (RMS) voltage. Ringing and event counts are affected, on the one hand, by the threshold and by hit definition time (HDT) and peak definition time (PDT) during the experiment. Therefore, the values of parameters to be measured considerably affect the degree of intensity of acoustic emission; while threshold, HDT and PDT are generally determined by experience and subject to the differences in environment and experimental materials, causing significant uncertainties. Based on the theoretical definition of ringing, ringing counts are not affected by parametric settings under particular thresholds and can indirectly reflect the degree of intensity of acoustic emission. Ge et al. [26] found in their study that ringing counts are of great certainty in comparison with other parameters, making it more suitable for determining the Kaiser points. The acoustic emission event is mainly reflected by the magnitude of energy released, which in turn is reflected by the sensor voltage. Thus, energy counts and RMS voltage can be used to judge the degree of intensity of acoustic emission, while RMS voltage is more suitable for continuous signals. As such, we preliminarily selected ringing counts and RMS voltage as parameters to determine Kaiser points.

Determining the Kaiser effect of acoustic emission relies upon the recurrence of effective acoustic emission phenomenon during the loading process. Most of the existing literature generally utilizes evident acoustic emission signals as a basis for the determination, which further gives rise to different determination methods such as the abrupt change points method, maximum curvature method, bitangent method, reloading method and integrative application of these methods. However, these methods all have their own limitations under different scenarios due to a lack of a clear definition of effective acoustic emission [29]. In his study, Ji et al. [13] quantitatively defined effective acoustic emission based on the standard of signal continuity and no less than 10 acoustic emission events when the load increases by 10%. Differences in experimental methods and acquisition parameters can cause the different frequencies of the occurrence of acoustic emission events, and the number of acoustic emission events alone cannot reflect the magnitude of energy released in the acoustic emission process. On this basis, this paper defines the effectiveness of acoustic emission by the following standards:

1) The acoustic emission signal is continuous during the process of load increase, that is, the continuity standard.

2) The location of the Kaiser point is determined intuitively on the cumulative curve of acoustic emission signals, and the average increase rate of the acoustic emission events within a certain area around both sides of the point is considered as the initiation point for effective acoustic emissions, which is also referred to as the increase rate standard of acoustic emission events.

On the basis of these standards, a concrete test tube (150 mm × 150 mm × 150 mm) with a maximum historical load of 800 kN was reloaded to 1000 kN. The parameters of cumulative ringing and RMS counts collected during the loading process were used to explain the method to identify Kaiser points. First, the cumulative acoustic emission parameter and load curve is shown in Fig. 9.

a) Cumulative ringing counts - pressure curve

$$y = 189.78e^{0.0067x}$$
$$R^2 = 0.9862$$

b) Cumulative RMS counts-pressure curve

$$y = 75.503e^{0.0068x}$$
$$R^2 = 0.9861$$

Figure 9 Cumulative ringing count/RMS-pressure curve

As can be preliminarily determined from Fig. 9, a load of about 780 kN was applied on the Kaiser point. With the 780 kN point as the center, determination intervals with widths of 100 kN, 200 kN and 300 kN were formed through an extension to both sides, that is, the intervals of [730 kN, 830 kN], [680 kN, 880 kN] and [630 kN, 930 kN]. Using the average increase rate of the acoustic emission parameter in each interval as the initiation point of effective acoustic emission, the parameters within the corresponding interval were fitted to a quadratic polynomial; the derivative of the quadratic polynomial is found, making it equal to the average increase rate of the acoustic emission parameter within the interval to be solved. Then solve the equation to obtain the Kaiser point, as shown in Fig. 10 and Tab. 3.

Fig. 10 shows that within different intervals selected after the preliminary determination of the Kaiser point, the cumulative acoustic emission curve fits well with the quadratic curve, and the smaller the selected interval, the better the fitting level, but the larger the effect of the initially determined value on the Kaiser point obtained. With an increase in the symmetric zone, the Kaiser point obtained increases gradually, and the extreme differences of the Kaiser point obtained respectively by cumulative ringing counts and cumulative RMS counts are 10kN(1.28%) and 5.46kN (0.68%). When it is difficult to preliminarily determine the Kaiser point, the selected fitting interval can be appropriately increased to reduce errors arising from the preliminary selection.
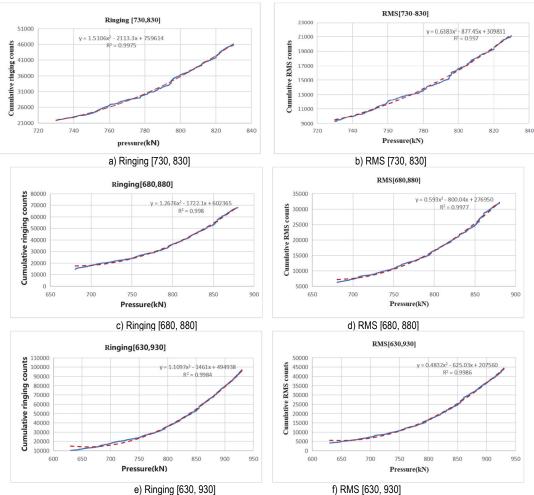
a) Ringing [730, 830]

b) RMS [730, 830]

c) Ringing [680, 880]

d) RMS [680, 880]

e) Ringing [630, 930]

f) RMS [630, 930]

Figure 10 Fitting curves with different intervals

Table 3 Kaiser points from different intervals

Interval	[730, 830]	[680, 880]	[630, 930]	Mean value / kN	Extreme difference
Cumulative ringing	778.67	784.24	788.67	783.86	10 kN (1.28%)
Felicity ratio	0.973	0.980	0.986	0.980	/
Cumulative RMS	780.11	782.38	785.57	782.69	5.46 (0.68%)
Felicity ratio	0.975	0.978	0.982	0.978	/

Fig. 10 shows that within different intervals selected after the preliminary determination of the Kaiser point, the cumulative acoustic emission curve fits well with the quadratic curve, and the smaller the selected interval, the better the fitting level, but the larger the effect of the initially determined value on the Kaiser point obtained. With an increase in the symmetric zone, the Kaiser point obtained increases gradually, and the extreme differences of the Kaiser point obtained respectively by cumulative ringing counts and cumulative RMS counts are 10 kN (1.28%) and 5.46 kN (0.68%). When it is difficult to preliminarily determine the Kaiser point, the selected fitting interval can be appropriately increased to reduce errors arising from the preliminary selection.

At present, Kaiser points are judged by the following methods: (1) Judging by the turning point on the impingement rate-stress curve [29]; (2) According to the signal continuity criterion and the increase criterion of the number of events, that is, acoustic emission signals are continuous, and there are more than 10 transmitted events when the load increases by 10% [30-32]; (3) Draw the cumulative count of AE and external force response curve, and judge by slope abrupt point [33]. Methods (1) and (3)

are intuitive, but there is no obvious turning point (mutation point) on the corresponding curve, which requires artificial judgment. Different people will get different results. Method (2): Although the judgment conditions are quantified, the judgment of events depends on hits. Several hits may or may not be judged as events by the system, so the number of events in the same acoustic emission experiment is uncertain. The method，that is studied in this paper is based on method (1) and method (3) preliminary judgment，combined with the signal continuity criterion, by function fitting of experimental data in the area near the initial judgment point, is used to correct the kaiser point. On the one hand, it effectively avoids the uncertainty of judgment caused by human factors in methods (1) and (3). On the other hand, it also makes up for the influence of uncertainty of event number in method (2) on kaiser's point judgment.

3.2 Kaiser Effect Analysis

The waveform files collected in the experiment presented in Section 2.2 were processed. The ringing counts were used as the parameter of the Kaiser effect

analysis. The Kaiser point was directly determined with the presence of an evident turning point, while a less Kaiser point was determined using the analytical method discussed in Section 3.1. Determination of Kaiser points for No. 1 - 4 beams is shown in Fig. 11 and Fig. 12 cumulative ringing counts-load (kN) curve, and the statistics of the Kaiser points is presented in Tab. 4.
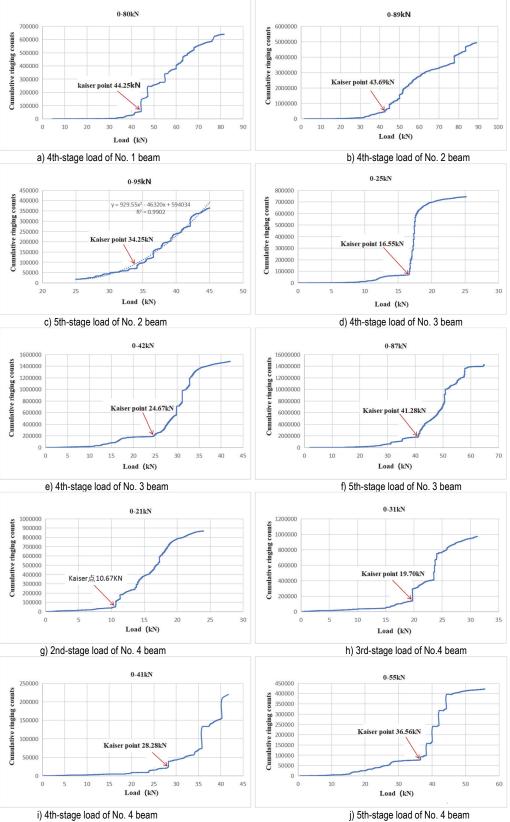

a) 4th-stage load of No. 1 beam

b) 4th-stage load of No. 2 beam

c) 5th-stage load of No. 2 beam

d) 4th-stage load of No. 3 beam

e) 4th-stage load of No. 3 beam

f) 5th-stage load of No. 3 beam

g) 2nd-stage load of No. 4 beam

h) 3rd-stage load of No.4 beam

i) 4th-stage load of No. 4 beam

j) 5th-stage load of No. 4 beam

Figure 11 Ringing count cumulative-load curve without failure

a) 5th-stage load of No. 1 beam

b) 6th-stage load of No. 1 beam

c) 6th-stage load of No. 2 beam

d) 7th-stage load of No. 2 beam

e) 5th-stage load of No. 3 beam

f) 6th-stage load of No. 4 beam
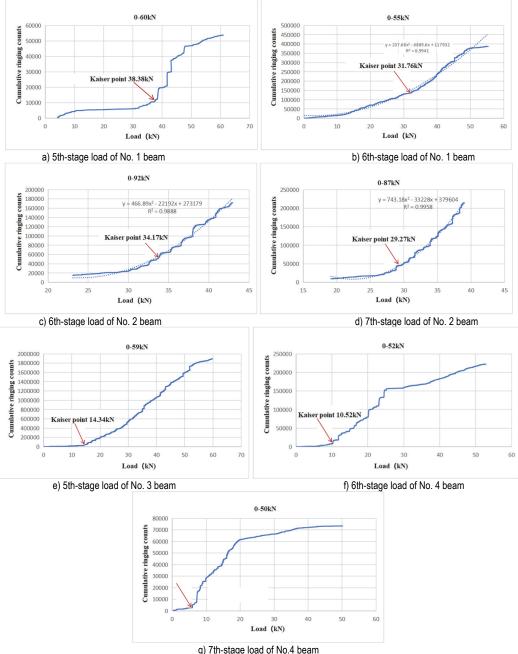

g) 7th-stage load of No.4 beam

Figure 12 Ringing count cumulative-load curve after failure

As can be seen from Fig. 11 and Fig. 12, there is an evident turning point when the cumulative ringing counts were used to determine the Kaiser point of the reinforced concrete beams. In some cases where the turning point is not evident, the method discussed in Section 3.1 was used to preliminarily determine the Kaiser point to identify analytical intervals, resulting in a good fitting between the curve drawn and the quadratic function. As such, the method is feasible to determine the Kaiser point. When ringing counts increase by leaps on the curve, it is generally accompanied by a slowly growing stage, which represents the increase stage of rebar tensile stress after the reinforced concrete beam fractures at the tensile region. With the cumulation of energy, another leap of growth in ringing counts appears when fractures recur. The load was re-applied on the beam when the ultimate bearing capacity was reached. As the new load was always smaller than the ultimate load, new tension fractures re-appear in the tensile

area of the beam, which are reflected by a relatively smooth ringing count-load curve, with no apparent leaps of growth in ringing counts, as differentiated from the acoustic emission characteristic curve of concrete compression test pieces.

As can be known from Tab. 4, before the historical extreme load reaches the ultimate bearing capacity, the Felicity ratio is invariably larger than 0.9 except for the 4th-stage load on No. 2 beam and 5th-stage load on No. 4 beam; additionally, with the load approaching the ultimate bearing capacity, the Kaiser point generally exhibits a pattern of appearing earlier. When the 5th-stage load on the No. 2 beam and No. 4 beam was applied, their historical extreme values respectively reached 93.68% and 74.55% of the ultimate bearing capacities. At this point, the beams were already near the failure stage. The initial defect tests showed that No. 2 and 4 beams had more evident defects in comparison with No. 1 and No. 3. When the load was re-

applied following the failure of beams, the Felicity ratio was 0.480 at maximum and 0.109 at a minimum across the 4 beams tested; the Kaiser effect weakened significantly, which generally exhibited the Felicity effect.

Table 4 Statistical table of Kaiser points for each beam

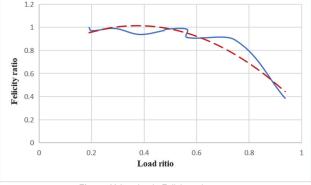| Beam No.	Item	2nd-stage / kN	3rd-stage / kN	4th-stage / kN	5th-stage / kN	6th-stage / kN	7th-stage / kN
No. 1	Historical extreme	45	45	45	80	80	/
	Kaiser point	/	/	44.25	38.38	31.76	/
	Felicity ratio	/	/	0.983	0.480	0.397	/
No. 2	Historical extreme	45	45	45	89	95	95
	Kaiser point	/	/	43.69	34.25	34.17	29.27
	Felicity ratio	/	/	0.971	0.385	0.360	0.308
No. 3	Historical extreme	16.6	25	42	87	/	/
	Kaiser point	16.55	24.76	41.28	14.34	/	/
	Felicity ratio	0.997	0.990	0.983	0.165	/	/
No. 4	Historical extreme	11	21	31	41	55	55
	Kaiser point	10.67	19.70	28.28	36.56	10.52	5.98
	Felicity ratio	0.970	0.938	0.912	0.892	0.191	0.109

Figure 13 Load ratio Felicity ratio curve

To examine the relationship between the Felicity ratio and ultimate bearing capacity, this paper defines the ratio of the current historical load extreme to ultimate bearing capacity as the load ratio, and the relationship between the load ratio and Felicity ratio was analyzed. The load ratio and Felicity ratio of each stage of load prior to failure of No. 1 - 4 beams was calculated and arranged in a descending order; the load ratio-Felicity ratio curve was drawn, as shown in Fig. 13. With an increase in load ratio, the Felicity ratio generally exhibits a decreasing trend. That is, the Felicity effect becomes stronger with an increase in load ratio. The outliers in the figure are mainly attributed to No. 2 and No. 4 beams, which may be caused by their initial defects.

The 2nd and 3rd stage loads of No. 1 and No. 2 did not reach the historical extremes, and thus it is impossible to judge whether their effective acoustic emission was restored from the curve. The cumulative ringing counts when different loads were taken from the ringing-load curve of each stage of loads on No. 1 through 4 beams are shown in Tab. 5.

As can be seen from Tab. 5, with an increase in the times of loads at the same load point, the resulting ringing counts decrease rapidly; as the load level increases, the velocity of decrease gradually declines. With initial structural defects, intense acoustic emission occurs when the load is reapplied. As can be seen from the 2nd stage loads of No. 2 and No. 4 beams, the acoustic emission counts reached 57%, 34% and 30% of those at the initial loading when historical extreme loads were not reached.

Table 5 Ringing statistics at the same load point

Beam No.	Load / kN	Item	1st stage	2 stage	3 stage	4th stage	5th stage
No. 1	15	Cumulative ringing	27183	1227	312	397	/
		Ratio	1.00	0.05	0.01	0.01	/
	30	Cumulative ringing	105351	15437	4732	1855	/
		Ratio	1.00	0.15	0.04	0.02	/
	45	Cumulative ringing	247403	/	/	145413	/
		Ratio	1	/	/	0.59	/
No. 2	15	Cumulative ringing	290151	166366	8922	6084	6375
		Ratio	1.00	0.57	0.03	0.02	0.02
	30	Cumulative ringing	1390519	471246	92074	51136	45179
		Ratio	1.00	0.34	0.07	0.04	0.03
	45	Cumulative ringing	1625687	/	/	934390	364961
		Ratio	1.00	/	/	0.57	0.22
No. 3	16.6	Cumulative ringing	236083	36251	22546	4470	18957
		Ratio	1.00	0.15	0.10	0.02	0.08
No. 4	11	Cumulative ringing	658650	198822	36366	2791	4781
		Ratio	1.00	0.30	0.06	0.004	0.007

Note: The ratios in the table refer to the ratio of ringing counts under each stage of load to the 1st-stage load

With an increase in the number of repeated loads, the acoustic emission appearing at the same load point drops rapidly. At the 3rd stage loads on No. 2 and No. 4 beams, the ratio dropped to 7% and 6%, respectively. Accordingly, the acoustic emission was not significant, reaching 15% at maximum, when repeated loads did not reach their historical extremes of No. 1 and No. 3 beams given their lesser defects. The test results show that in the low stress area, repeated loads have a significant effect on the weakening of the degree of intensity of acoustic emission, while such an effect gradually decreases in the high stress area. As such, repeated loads not exceeding the historical load extremes in the low stress area play a positive effect on the generation of the Kaiser effect. The test results also indicate that when judging whether effective acoustic emission is produced, relying upon the turning point on

curves or the number of acoustic emission events has its limitations. Instead, curve changes and the growth rate of acoustic emission should both be taken into account and the current intensity of acoustic emission should be compared with that of the earlier-stage loads. For example, when the 2nd stage load on the No. 2 beam reached 15 kN, its acoustic emission event ratio was 57%. Although the maximum value of the load (15 kN) did not reach the historical extreme (45 kN), the authors consider it plausible to determine that an evident acoustic emission had occurred. When the 3rd stage load reached 15 kN, the ratio of acoustic emission events dropped to 3%; when the 4th stage load exceeded the historical extreme, the Kaiser point was 43.69 kN.

4 CONCLUSIONS

Four-point bending experiment was conducted on four reinforced concrete simply supported beams. According to the signal continuity criterion, the quadratic fitting function based on experimental data near the Kaiser point was utilized through the analysis of acoustic emission parameters, thus correcting the Kaiser point. The Kaiser effect under different loading mechanisms of reinforced concrete was explored. The following conclusions were obtained:

(1) Ring-down count or root-mean-square (RMS) voltage count was determined as the analysis parameter. According to the signal continuity criterion, the quadratic fitting function based on experimental data in the interval near the initial judgment point was utilized. Taking the average increasing rate of acoustic emission signals within this interval as the indicator for acoustic emission recovery, the Kaiser point was corrected to avoid the influence of human factors and uncertainty of acoustic emission events on commonly used methods, and to achieve better certainty and operability of the Kaiser point.

(2) As the load increased, the acoustic emission signal of reinforced concrete was stable during the accumulation stage of stress and damage. When micro damage accumulated and macroscopic cracking occurred, the acoustic emission signal increased by leaps. The higher the degree of cracking, the higher the degree of increasing by leaps. The signal slowly increased once the load exceeded the ultimate bearing capacity of the beams. Increasing by leaps would almost never occur again. The generation time and crack degree of the beams can be determined through acoustic emission signal analysis, thus providing a basis for concrete damage monitoring.

(3) The reinforced concrete simply supported beams exhibited a significant Kaiser effect under four-point bending. As the stress increased, the Felicity ratio first slowly increased and then decreased. Once the load ratio reached 0.6, the Felicity ratio decreased to below 0.95, and the simply supported beams presented a significant Felicity effect. This trend can provide a basis for determining the historical stress state and ultimate bearing capacity of beams based on the Kaiser effect.

(4) If the historical load was not higher than 50% of the ultimate stress, repeated loading would make the Kaiser point clearer and enhance the Kaiser effect. The acoustic emission characteristics of the low stress stage were enhanced by the initial defect, in addition, the initial defect

also leads to the decrease of kaiser effect and the advance of felicity effect. As the load increased, micro damage gradually merged and strengthened. This influence would gradually weaken or even disappear. Therefore, it is possible to utilize the Kaiser effect to determine the historical maximum load of the bridge. These results provide a basis for detecting existing damage and evaluating historical maximum load of Bridges by using AE characteristics and the Kaiser effect.

The acoustic emission signals used for this research were collected from the new components. During the experiment, the effect of material aging over service time on acoustic emission signals was not considered. To ensure the applicability of research results to existing structures, it is necessary to further explore the influence of material aging on acoustic emission signals and identify the historical load limits of existing structures.

5 REFERENCES

[1] Shen, G. T. (2005). *Acoustic emission detection technology and its application*. Beijing: Kexue Publishing House.

[2] Yi, Y., Woods, R., Ting, L. K., & Cowan, C. F. N. (2005). High speed FPGA-based implementations of delayed-LMS filters. Journal of VLSI signal processing systems for signal. *Image and Video Technology*, *39*(1), 113-131. https://doi.org/10.1023/B:VLSI.0000047275.54691.be

[3] Katsuyama, K. (1996). Application of acoustic emission (AE) technology. *Beijing: Press Metall. Industry*.

[4] Jin, X. H. & Zheng, J. Y. (2021). Acoustic emission features of anthracite under the influence of loading rate. *Annales de Chimie-Science des Matériaux*, *45*(5), 393-397. https://doi.org/10.18280/acsm.450505

[5] Kaiser, E. J. (1950). *A study of acoustic phenomena in tensile test*. PhD Dissertation. Technical University of Munich, 9.

[6] Yang, R. F. & Ma, T. H. (2006). A Study on the Applications of Acoustic Emission Technique. *Journal of North University of China (Natural Science Edition)*, *27*(5), 456-461.

[7] Zhao, K., Xiang, W., Zeng, P., Yang, D., Wu, W., Gong, C., & Yang, X. (2021). Research status and prospect of kaiser effect in rock acoustic emission. *Metal Mine*, *50*(1), 94-105.

[8] Liu, T., Mao, H. L., Huang, Z. F., & Mao, H. Y. (2017). Chaotic characteristics of Kaiser effect of metal acoustic emission. *Journal of Vibration and Shocka*, *36*(12), 50-54.

[9] Rusch, H. (1959). Physical Problems in the Testing of Concrete (Physikalische Fragen der Betonprufung). *Zement-Kalk-Gips*, *12*(1), 15-25.

[10] Yang, C. Z., Han, J. D., & Wang, S. G. (2016). Review on application of acoustic emission technique in reinforced concrete. *Concrete*, *2016*(10), 152-157.

[11] McCabe, W. M., Koerner, R. M., & Lord, A. E. (1976). Acoustic emission behavior of concrete laboratory specimens. *Journal of the American Concrete Institute*, *73*(7), 255-260.

[12] Watanabe, T., Nishibata, S., Hashimoto, C., & Ohtsu, M. (2007). Compressive failure in concrete of recycled

aggregate by acoustic emission. *Construction and Building Materials*, *21*(3), 470-476. https://doi.org/10.1016/j.conbuildmat.2006.04.002

[13] Ji, H. G. & Li, Z. D. (1996). Experimental study on the relationship between felicity effect and kaiser effect in concrete material. *Applied Acoustics*, *16*(6), 30-33.

[14] Yuan, R. F., Li, Y. H., & Zhao, X. D. (2007). Experimental Verification and Theoretical Analysis on Felicity Effect of Acoustic Emission in Concrete. *Key Engineering Materials, 353-358*, 2333-2336. https://doi.org/10.4028/www.scientific.net/KEM.353-358.2333

[15] Wu, S. X., Zhang, S. X., & Shen, D. J. (2008). An experimental study on Kaiser effect of acoustic emission in concrete under uniaxial tension loading. *China Civil Engineering Journal*, *41*(4), 31-39.

[16] Wang, B. L., Yan, S. R., Huang, T. Y., & Chu, F. M. (2022). Acoustic emission characteristics and Kaiser effect of recycled concrete. *Nondestructive Testing*, *2022*(04), 40-44.

[17] Yu, J., Pi, Y. J., & Qin, Y. J. (2021). Acoustics emission characteristics of damage of recycled aggregate concrete under cyclic loading. *Materials Reports*, *35*(13), 13011-13017.

[18] Men, J. J., Zhu, L., Li, H., & Wang, X. D. (2015). Experimental research on the acoustic emission detecting parameters and mechanical behaviors for reinforced concrete structure. *Journal of Xi'an University of Architecture & Technology (Natural Science Edition)*, *47*(06), 793-798.

[19] Fan, X. Q., Hu, S. W., & Lu, J. (2015). Acoustic emission characteristics identification and related parameters influence of reinforced concrete fracture process. *Science China (Technological Sciences)*, *45*(08), 849-856. https://doi.org/10.1360/N092014-00056

[20] Yu, D. K. (2016). *Analysis of damage evolution of reinforced concrete beams based on acoustic emission and BP neural network*. Jiangsu University.

[21] Chen, Z. G. (2018). *Identification and degradation assessment of reinforced concrete damage based on acoustic emission technology*. Zhejiang University.

[22] Rasheed, M. A., Prakash, S. S., Raju, G., & Kawasaki, Y. (2018). Fracture studies on synthetic fiber reinforced cellular concrete using acoustic emission technique. *Construction and Building Materials*, *169*, 100-112. https://doi.org/10.1016/j.conbuildmat.2018.02.157

[23] Nguyen-Tat, T., Ranaivomanana, N., & Balayssac, J. P. (2018). Characterization of damage in concrete beams under bending with Acoustic Emission Technique (AET). *Construction and Building Materials*, *187*, 487-500. https://doi.org/10.1016/j.conbuildmat.2018.07.217

[24] Shi, T. X. (2021). *Research on damage characteristics of high strength concrete specimen based on acoustic emission technology*. XIAN: Xi`an University of Architecture and Technology.

[25] Shield, C. K. (1997). Comparison of acoustic emission activity in reinforced and prestressed concrete beams under bending. *Construction and Building Materials*, *11*(3), 189-194. https://doi.org/10.1016/S0950-0618(97)00036-6

[26] Ge, R. D., Liu, M. J., & Zhao, Y. L. (2011). Determination of kaiser point in reinforced concrete beam under cyclic loading. *Journal of Guilin University of Technology*, *31*(4), 554-557.

[27] Xiong, Y. & Cheng, L. (2015). Study of characteristics of acoustic emission during entire loading tests of concrete and its application. *Journal of Building Materials*, *18*(3), 380-386.

[28] Chen, S. D., Shi, Q. Y., Yang, F., Cao, L. L., & Yang, B. X. (2014). Study of injury classification of prestressed concrete beams. *Science Technology and Engineering*, *14*(18), 110-117.

[29] Lavrov, A. (2001). Kaiser effect observation in brittle rock cyclically loaded with different loading rates. *Mechanics of materials*, *33*(11), 669-677. https://doi.org/10.1016/S0167-6636(01)00081-3

[30] Iida, T., Watanabe, H., Tomoda, Y., & Ohtsu, M. (2000). Damage estimation of concrete core by AE rate process analysis. *Proc. of the Japan Concrete Institute*, *22*(1), 271-276.

[31] Zhu, H. P., Xu, W. S., Chen, X. Q., & Xia, Y. (2008). Quantitative concrete-damage evaluation by acoustic emission information and rate-process theory. *Engineering Mechanics*, *2008*(1), 186-191.

[32] Chen, Q. X. (1998). *Rock mechanics and tectonic stress field analysis*. Beijing: Geology Press.

Contact information:

Yongfeng XU
School of Traffic and Transportation, Shijiazhuang Tiedao University, Shijiazhuang 050043, Hebei, China
Hebei Institute of Civil Engineering and Architecture, Zhangjiakou 075000, Hebei, China
Hebei Provincial Key Laboratory of Civil Engineering Diagnosis, Reconstruction and Disaster Resistancer, Zhangjiakou 075000, Hebei, China
E-mail: xyf1506@hebiace.edu.cn

Hailong WANG
School of Traffic and Transportation, Shijiazhuang Tiedao University, Shijiazhuang 050043, Hebei, China
Hebei Institute of Civil Engineering and Architecture, Zhangjiakou 075000, Hebei, China
Hebei Provincial Key Laboratory of Civil Engineering Diagnosis, Reconstruction and Disaster Resistancer, Zhangjiakou 075000, Hebei, China
E-mail: wanghl@hebiace.edu.cn

Tengfei HE
(Corresponding author)
Hebei Institute of Civil Engineering and Architecture, Zhangjiakou 075000, Hebei, China
Hebei Provincial Key Laboratory of Civil Engineering Diagnosis, Reconstruction and Disaster Resistancer, Zhangjiakou 075000, Hebei, China
E-mail: htf037@126.com

Jiajun MA
Hebei Institute of Civil Engineering and Architecture, Zhangjiakou 075000, Hebei, China
E-mail: hhh-0002@163.com

Pengfei ZHAO
Hebei Institute of Civil Engineering and Architecture, Zhangjiakou 075000, Hebei, China
E-mail: q787234141@163.com

Anquan JI
Hebei Institute of Civil Engineering and Architecture, Zhangjiakou 075000, Hebei, China
E-mail: han5814@163.com

Lei LIU
Hebei Institute of Civil Engineering and Architecture, Zhangjiakou 075000, Hebei, China
E-mail: llnl1998@163.com

Yang LIU
Hebei Institute of Civil Engineering and Architecture, Zhangjiakou 075000, Hebei, China
E-mail: 17735742682@163.com